Mechanics of Materials 140 (2020) 103221

Contents lists available at ScienceDirect

Mechanics of Materials

journal homepage: www.elsevier.com/locate/mechmat

Research paper

# Studying hydrogen effect on the core structure and mobility of dislocation in nickel by atomistically-informed generalized Peierls–Nabarro model

Zhouqi Zheng[a], Shuang Liang[a], Yaxin Zhu[a,b,*], Minsheng Huang[a,b], Zhenhuan Li[a,b,*]

[a] Department of Mechanics, Huazhong University of Science and Technology, Wuhan, 430074, China
[b] Hubei Key Laboratory of Engineering Structural Analysis and Safety Assessment, 1037 Luoyu Road, 430074, Wuhan, China

ARTICLE INFO

*Keywords:*
Hydrogen-dislocation interaction
Stacking fault energy
Peierls–Nabarro model
Dislocation core
Peierls stress

ABSTRACT

Hydrogen (H) atoms in the metallic crystalline lattice interact with the pre-existing dislocations and then remarkably affect the plastic deformation of metals. Thereby quantitatively characterizing the H-dislocation interaction is of great importance for understanding H-induced plasticity and failure. Most of the previous studies have focused on the long-range interaction between hydrogen and dislocation, but rarely considered the short-range interaction, especially the hydrogen effect on the dislocation core structure. Here, with the aid of the H-affected γ-surface calculated from atomistic modeling, an atomistically-informed generalized Peierls–Nabarro model is employed to study the hydrogen effect on the core structure of dislocation, the recombination energy of the extended screw dislocation, and the Peierls stress in nickel. Our results show that, on the one hand, hydrogen can decrease the stable stacking fault energy, leading to the increase of the stacking fault width for both extended edge and screw dislocations. Consequently, the recombination energy of extended screw dislocation is increased, indicating that hydrogen can suppress the cross-slip of screw dislocation and facilitate the slip planarity observed frequently in experiments. On the other hand, hydrogen can increase the unstable stacking fault energy, implying that hydrogen can inhibit the nucleation of partial dislocations. Moreover, hydrogen in the dislocation core increases the Peierls stress and thus increases dislocation slip resistance. Finally, quantitative relations between the Peierls stress and hydrogen concentration are given. These results are of great significance for understanding the H-affected dislocation plasticity mechanisms, and can be used for quantifying the hydrogen effect on dislocation dynamics.

## 1. Introduction

Hydrogen, as a clean and renewable energy, can offer an effective pathway to decarbonize the energy system and to mitigate the energy crisis (Sharma and Ghoshal, 2015). However, the production, transportation and utilization of hydrogen suffer from hydrogen embrittlement (HE) threat, which is one of the most common failure modes due to extreme environment (Barrera et al., 2018; Robertson et al., 2015). The detrimental effects of hydrogen on the mechanical properties of metals were first reported in 1875 by Johnson (Johnson, 1875). Since then, enormous studies on HE have been made and several mechanisms have been proposed, including hydride formation and cleavage (HFC) (Gahr et al., 1977; von Pezold et al., 2011), hydrogen-enhanced decohesion (HEDE) (Nagao et al., 2018; Oriani and Josephic, 1974), hydrogen-enhanced localized plasticity (HELP) (Ferreira et al., 1998; Robertson, 1999), hydrogen-enhanced strain-induced vacancy formation (HESIV) (Nagumo and Takai, 2019) and so on, trying to explain the HE phenomenon. Among these mechanisms, the operative ones depend not only on the intrinsic microstructure of metals, but also on the loading type, hydrogen concentration and other external conditions. Thereby the exact mechanism of the premature failure due to the presence of hydrogen is still in debate, since the underlying atomic processes remain unclear. The micro- even nano-scaled details are in urgent to figure out the role that hydrogen plays during the deformation and failure processes. With the development of SEM/TEM technique, the observations in micro- and nano-scales make it possible to investigate the HE mechanism more precisely. During many years, HE has been considered to relate insignificantly to the plastic deformation. However, the recent TEM observations show that there exist extensive dislocation substructures beneath the intergranular fracture surfaces in Ni and iron deformed in H environment (Martin et al., 2012; Wang et al., 2014). Since dislocation is the main carrier of plastic deformation in metals, how hydrogen affects dislocation motion is therefore a key scientific question in understanding the H-induced

* Corresponding authors.
*E-mail addresses:* yxzhu2006@hust.edu.cn (Y. Zhu), zhenhuanli@hust.edu.cn (Z. Li).

https://doi.org/10.1016/j.mechmat.2019.103221
Received 26 June 2019; Received in revised form 23 October 2019; Accepted 23 October 2019
Available online 24 October 2019
0167-6636/ 

failure mechanisms and depicting the H-affected dislocation evolution.

Due to the complexity of the H-dislocation interaction, the effect of hydrogen on the dislocation mobility remains in debate. On the one hand, Robertson et al. reported that hydrogen can enhance the dislocation mobility based on their TEM observation (Ferreira et al., 1998; Robertson, 1999). In order to explain this experimental phenomenon, some scholars suggested that hydrogen atmospheres formed around dislocations could shield the elastic interactions between dislocations and various defects (Cai et al., 2014; Sofronis, 1995; Song et al., 2019). Due to strong shield effect by the H atmospheres, the interactions between dislocations and between dislocations and other defects become weak and the dislocation mobility increases. In general, the shielding effect becomes noticeable only at very high background H concentration (Song et al., 2019; von Pezold et al., 2011). On the other hand, based on the atomic calculations, Song and Curtin (Song and Curtin, 2014) reported that the H atmospheres could reduce rather than enhance the mobility of edge dislocations in α-Fe, which is consistent with the solute drag theory (Cottrell and Bilby, 1949). Recently, Xie et al. (2016) conducted in-situ environmental TEM tests and also observed that the mobile dislocations in Al became immobile under hydrogen environment, which was attributed to the interaction between mobile dislocations and hydrogen-vacancy complexes (Li et al., 2015; Zhu et al., 2017). In fact, hydrogen has two effects on dislocation motion. One is the long-range effect and the other is the short-range effect. Those H atoms trapped by dislocation stress field govern the long-range effect, which is responsible for the shielding effect mentioned above and is usually used to explain HELP mechanism. However, those H atoms lying within the dislocation core govern the short-range effect, which is a key intrinsic factor and is responsible for dislocation motion, dislocation nucleation, and dislocation emission and so on. To our knowledge, in previous studies, more attention has been paid to the long-range effect of H on dislocation motion but less to the short-range effect. In reality, dislocation motion and evolution in the H-charged metals depend not only on the long-range effect but also on the short-range effect.

As we know, H atoms in metals can stay in lattices and can also be trapped by various defects (Oriani, 1970). It is difficult to observe experimentally the details of the short-range interaction between dislocations and H atoms, so atomistic simulation is usually adopted although it cannot capture hydrogen diffusion in metals due to time scale limitation. Lu et al. (2001) conducted ab initio calculations and found that hydrogen could enhance dislocation mobility but suppress the cross-slip of dislocation in Al. Similar effect of hydrogen on the cross-slip process of an extended screw dislocation in Ni was also found by using the nudged elastic band (NEB) method (Wen et al., 2004). First principle study of the screw dislocation in BCC iron showed that hydrogen could decrease the kink nucleation enthalpy while increase the kink migration enthalpy, implying that hydrogen either enhances or reduces the screw dislocation mobility, depending strongly on the hydrogen concentration (Itakura et al., 2013). Atomic-scale investigation of hydrogen atmospheres on the edge dislocation mobility in α-Fe showed that the hydrogen atmosphere could hinder the motion of edge dislocation (Song and Curtin, 2014). To study the effect of the H-defect complexes on dislocation motion, the short-range interactions between dislocation and H-defect complexes were modeled using molecular dynamic (MD) method, showing that the hydrogen-vacancy complex could serve as an obstacle to pin the edge dislocation in α-Fe (Li et al., 2015; Zhu et al., 2017). Although atomistic simulation can catch some details of the H-dislocation interactions, the reliability of the computational results has been questionable due to the limitation of temporal and spatial scales. Some new methods and models should be developed to study them.

Hydrogen atoms can be trapped by dislocation, which can heavily change dislocation core structure. Therefore, how to characterize the effect of hydrogen on dislocation core structure is of great significance for quantitatively studying the short-range H-dislocation interaction. To address it, a suitable dislocation model is needed. Due to singularity of the Volterra dislocation model (Hirth and Lothe, 1992), it is difficult to characterize quantitatively the effect of hydrogen on the dislocation core structure. In this paper, the Peierls–Nabarro (P–N) dislocation model with nonsingular core is adopted to study the hydrogen effect on dislocation core structure and its mobility. The original P-N model is based on the balance between the elastic stress field due to distributional Burgers vector and the restoring stress field due to the atomic misfit (Nabarro, 1947; Peierls, 1940). However, it is only valid for very wide dislocation core and for the pure edge or screw dislocations. These restrictions can be eliminated by considering the dislocation energy as a functional of the misfit function (Schoeck, 2005). The total energy of the P-N model includes the elastic energy which can be obtained analytically, and the misfit energy which can be evaluated numerically with generalized stacking fault energy (GSFE), i.e. the γ-surface (Vítek, 1968). The γ-surface can be determined accurately from ab initio calculation or MD simulation. Therefore, the generalized P–N model has the virtue of incorporating atomistic interactions into continuum models. By minimizing the total energy with respect to the misfit function, the dislocation core structure, the recombination energy for cross-slip and the Peierls stress can be obtained through the generalized P-N model, straightforwardly (Bulatov and Cai, 2006; Szajewski et al., 2017).

The manuscript is organized as follows: the illustration of the dissociated dislocation, the framework of the generalized P–N model, the computational details of the H-affected γ-surface, the recombination energy and the Peierls stress are given in Section 2; some numerical results are then presented in Section 3; at last, the paper ends with some main conclusions in Section 4.

## 2. Theory and implementation

### 2.1. Shockley partial dislocation and stacking fault in FCC crystals

A perfect dislocation with Burgers vector of $\mathbf{b} = a/2\,[\bar{1}01]$ on the (111) slip plane in FCC crystals prefers to dissociate into two Shockley partial dislocations separated by an intrinsic stacking fault (SF) between them, as illustrated in Fig. 1. The orthogonal coordinate system is adopted with the X-axis along the $[1\bar{2}1]$ direction, the Z-axis along the $[\bar{1}01]$ direction (i.e. the direction of the Burgers vector **b**) and the Y-axis along [111] direction (i.e. the slip plane normal). A perfect edge dislocation with line direction parallel to the X-axis dissociates into two 60° mixed partial dislocations as shown in Fig. 1(a), while a perfect screw dislocation with line direction parallel to Z-axis dissociates into two 30° mixed partial dislocations as shown in Fig. 1(b). The dissociation equation for both edge and screw dislocations can be expressed as:

$$\begin{cases} \mathbf{b} = \mathbf{b}_{p1} + \mathbf{b}_{p2} + \mathrm{SF} \\ \frac{a}{2}[\bar{1}01] = \frac{a}{6}[\bar{1}\bar{1}2] + \frac{a}{6}[\bar{2}11] + \mathrm{SF} \end{cases} \tag{1}$$

Since the Burgers vectors $\mathbf{b}_{p1}$ and $\mathbf{b}_{p2}$of the two partial dislocations are angled at 60° from each other, they repel each other due to their elastic interaction. On the other hand, there is a stable SF with energy $\gamma_{ssf}$ per unit area between the two partial dislocations, providing an attractive force trying to pull the two partial dislocations together. When repulsion and attraction are in balance, the equilibrium separation can be obtained by (Hirth and Lothe, 1992)

$$\frac{d_{eq}}{|\mathbf{b}|} = \left[\frac{\mu|\mathbf{b}|(2-\nu)}{24\pi\gamma_{ssf}(1-\nu)}\right]\left[1 - \frac{2\nu\cos(2\theta)}{2-\nu}\right] \tag{2}$$

where $\mu$ is shear modulus, $\nu$ the Poisson's ratio, and $\theta$ the intersection angle between dislocation line and the Burgers vector direction (0° for the screw dislocation or 90° for the edge dislocation). The isotropic elastic constants $\mu$ and $\nu$ can be calculated by three cubic elastic

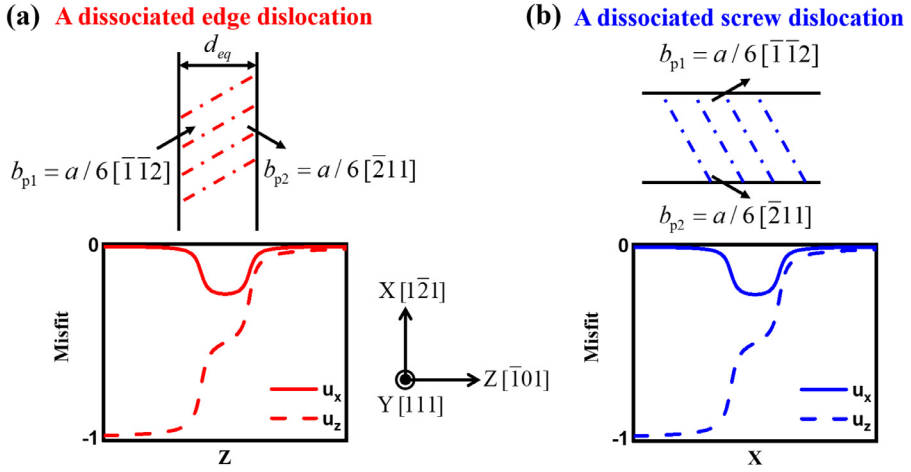


**Fig. 1.** Diagram of a perfect $a/2$ [$\bar{1}$01] dislocation splitting into two Shockley partial dislocations separated by a stacking fault ribbon on the (111) slip plane in FCC crystals. (a) The edge dislocation line is parallel to the X-axis while (b) the screw dislocation line is parallel to the Z-axis. The misfit functions for both edge and screw dislocations are also illustrated.

constants, with $C_{11} = 246.4$ MPa, $C_{12} = 147.3$ MPa and $C_{44} = 124.8$ MPafor Ni (Angelo et al., 1995). In order to consider the anisotropy of FCC crystals, Szajewski et al. (2018) suggested taking Hill's average elastic constants, which can describe the dislocation core for both edge and screw dislocations reasonably. Unless otherwise stated, the elastic constants used for further calculations are all determined by Hill's method.

### 2.2. The generalized Peierls–Nabarro model

For a straight screw dislocation with its line along the Z-axis, its core structure can be described by a two dimensional misfit function $\mathbf{u}(x) = \{u_x(x), u_z(x)\}$ (for an edge dislocation, the misfit function should be $\mathbf{u}(z) = \{u_x(z), u_z(z)\}$), which can be computed by the relative displacements of atoms just above and below the slip plane, as illustrated in Fig. 1. In order to keep conservation of the Burgers vector, the misfit function must satisfy the following boundary conditions:

$$\begin{cases} u_x(+\infty) = u_x(-\infty) = 0 \\ u_z(+\infty) - u_z(-\infty) = b \end{cases} \tag{3}$$

where $b = a/\sqrt{2}$ is the magnitude of the Burgers vector. Then, we can calculate the misfit density $\boldsymbol{\rho}(x) = d\mathbf{u}(x)/dx$, which describes the distribution of the Burgers vector on the slip plane (Eshelby, 1949).

In the classical Peierls-Nabarro (P–N) model (Nabarro, 1947; Peierls, 1940), the misfit function can be determined by the balance between the elastic stress due to the distribution of the Burgers vector and the restoring stress due to the atomic misfit. When the misfit vector is limited to have only one non-zero component $u_z$ along the Burgers vector direction and the restoring force is assumed to be sinusoidal, the misfit function and misfit density are given by (Hirth and Lothe, 1992)

$$\begin{cases} u_z(x) = \frac{b}{\pi}\arctan\left(\frac{x}{w}\right) - \frac{b}{2} \\ \rho_z(x) = \frac{du_z}{dx} = \frac{b}{\pi}\frac{w}{x^2 + w^2} \end{cases} \tag{4}$$

where $w$ denotes the dislocation core width.

When considering an extended dislocation whose misfit vector has both $u_x$ and $u_z$ components, the misfit function should be varied. Taking an extended screw dislocation for example, it has both edge and screw components of the Burgers vector, which are denoted by $b_e = \sqrt{3}b/6$ and $b_s = b/2$, respectively. Motivated by the original P–N model, the extended screw dislocation can be represented by superposition of the P–N type dislocations as (Bulatov and Cai, 2006):

$$\begin{cases} u_x(x) = \frac{b_e}{\pi}\left[\arctan\left(\frac{x - x_e^{(1)}}{w_e}\right) - \arctan\left(\frac{x - x_e^{(2)}}{w_e}\right)\right] \\ u_z(x) = \frac{b_s}{\pi}\left[\arctan\left(\frac{x - x_s^{(1)}}{w_s}\right) + \arctan\left(\frac{x - x_s^{(2)}}{w_s}\right)\right] - \frac{b}{2} \end{cases} \tag{5}$$

In the above equations, $x_e^{(i)}$ and $x_s^{(i)}$ are the positions of the edge and screw components of each partial dislocation ($i = 1, 2$), respectively, with $w_e$ and $w_s$ being the corresponding partial dislocation core widths. The superscript represents the two partial dislocations, while the subscript denotes either edge or screw components. The equilibrium separations for the edge ($d_e = x_e^{(1)} - x_e^{(2)}$) and screw ($d_s = x_s^{(1)} - x_s^{(2)}$) components should be the same, so we can take either of the two separations as the equilibrium spacing ($d_{eq}$) between the two partial dislocations. In addition, the center of the dislocation is determined by $x_e^c = (x_e^{(1)} + x_e^{(2)})/2$ for the edge components and $x_s^c = (x_s^{(1)} + x_s^{(2)})/2$ for the screw components, respectively. The extended dislocation determined by Eq. (5) yields shear stresses on the slip plane due to its edge and screw components of the Burgers vector, which can be expressed as follows (Hirth and Lothe, 1992):

$$\begin{cases} \tau_{yx}^0(x) = \frac{\mu b_e}{2\pi(1-\nu)}\left[\frac{x - x_e^{(1)}}{(x - x_e^{(1)})^2 + w_e^2} - \frac{x - x_e^{(2)}}{(x - x_e^{(2)})^2 + w_e^2}\right] \\ \tau_{yz}^0(x) = \frac{\mu b_s}{2\pi}\left[\frac{x - x_s^{(1)}}{(x - x_s^{(1)})^2 + w_s^2} + \frac{x - x_s^{(2)}}{(x - x_s^{(2)})^2 + w_s^2}\right] \end{cases} \tag{6}$$

For an extended edge dislocation, the misfit function should be replaced by $\mathbf{u}(z)$ and the shear stresses can be deduced similarly.

The total energy of the extended dislocation is a functional of the misfit function $\mathbf{u}$, which comprises of an elastic strain energy $E_{\text{elastic}}$ due to the distribution of the Burgers vector, a misfit potential $E_{\text{misfit}}$ due to the relative displacements of atoms immediately adjacent to the slip plane, and the work $E_{\text{applied}}$ due to the externally applied stress (Bulatov and Cai, 2006):

$$E_{\text{total}} = E_{\text{elastic}} + E_{\text{misfit}} + E_{\text{applied}} \tag{7}$$

In the generalized P–N model, the whole crystal, excluding the two lattice planes just above and below the slip plane, is treated as a linear elastic medium. Applying the displacement field of Eq. (5) to the surfaces of the continua yields an elastic deformation. Then, the elastic strain energy can be integrated along the slip plane by using Eqs. (5) and (6):

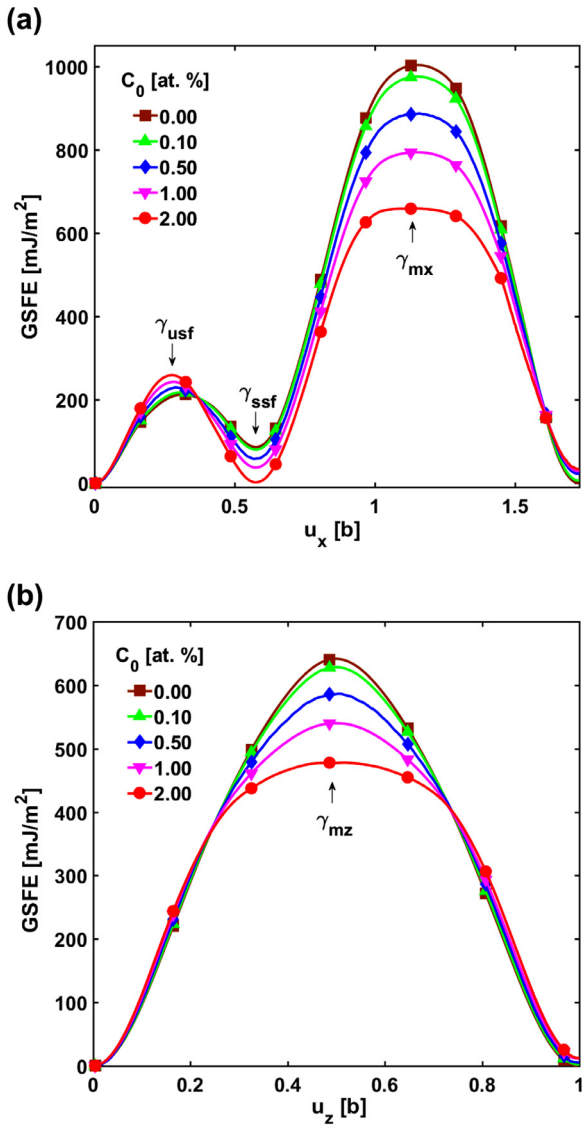


**Fig. 2.** The H-affected GSFE curves on the (111) slip plane along (a) the $[1\bar{2}1]$ and (b) the $[\bar{1}01]$ directions, respectively, which are obtained by atomic simulations.

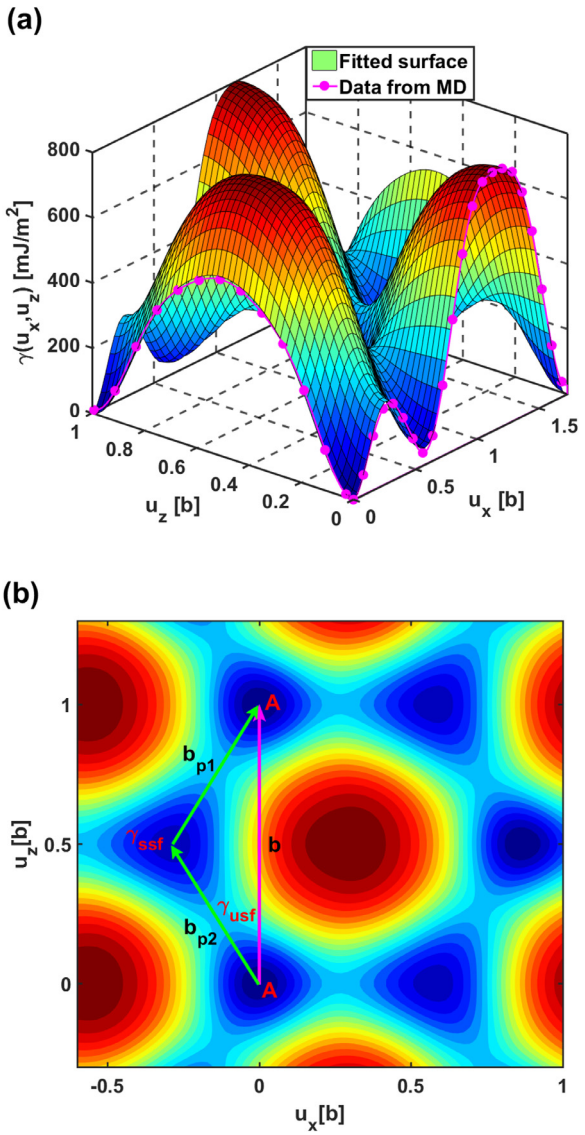


**Fig. 3.** (a) The fitted γ-surface at the H concentration of 1.0 (at.%), where the red circles represent the GSFE curves calculated by atomistic modellings. (b) The corresponding contour of GSFE.

$$E_{\text{elastic}} = \int_{-R}^{R} (\tau_{yx}^{0}(x)u_x(x) + \tau_{yz}^{0}(x)u_z(x))dx = \frac{\mu b_s^2}{4\pi}\left[4\ln\left(\frac{R}{2w_s}\right) - \ln\left(1 + \frac{d_s^2}{4w_s^2}\right)\right] + \frac{\mu b_e^2}{4\pi(1-\nu)}\ln\left(1 + \frac{d_e^2}{4w_e^2}\right) \tag{8}$$

where $R$ is the outer cut-off radius, being over 5000$b$ in our calculations to achieve numerical convergence (Bulatov and Cai, 2006).

Imaging that a perfect FCC crystal is divided by its slip plane, the upper half is sheared rigidly with respect to the lower one by a two dimensional uniform misfit vector**u**. Such procedure doesn't produce elastic energy, because there is no elastic deformation from the perspective of continuum scale. However, it indeed changes the relative positions of real atoms immediately adjacent the slip plane, inducing surplus energy per unit area of the cut plane. This energy is the so-called generalized stacking fault energy (GSFE) γ, i.e. the γ-surface (Vítek, 1968). Since the misfit only occurs at the actual atomic rows, the misfit potential should be summed discretely only at the positions of the atoms just above and below the slip plane (Bulatov and Cai, 2006; Bulatov and Kaxiras, 1997). Therefore, we can write the misfit energy as:

$$E_{\text{misfit}} = \sum_{n=-N}^{N} \gamma(u_x(na_p), u_z(na_p))a_p \tag{9}$$

where $a_p$ is the lattice period along the dislocation line normal, which is $b/2$ for an edge dislocation and $\sqrt{3}b/2$ for a screw dislocation, and $N = R/a_p$ denotes the half number of atomic rows used in our calculations. The construction of the GSFE surface $\gamma(\mathbf{u})$ is depicted below in Section 2.3.

Two external shear stresses on the glide plane are considered. One is parallel to the Burgers vector, i.e. the glide stress $\tau_{yz}$, which can drive the dislocation to glide on the slip plane. The other is perpendicular to the Burgers vector, i.e. the Escaig stress $\tau_{yx}$, which can change the equilibrium separation between the partial dislocations. Thus, the work done by the two externally applied stresses can be described by

$$E_{\text{applied}} = -\tau_{yx}\sum_{n=-N}^{N} u_x(na_p)a_p - \tau_{yz}\sum_{n=-N}^{N} u_z(na_p)a_p \tag{10}$$

The equilibrium dislocation geometry under certain externally applied stresses can be determined by minimizing the total energy in Eq. (7) with respect to the six unknown parameters in the misfit

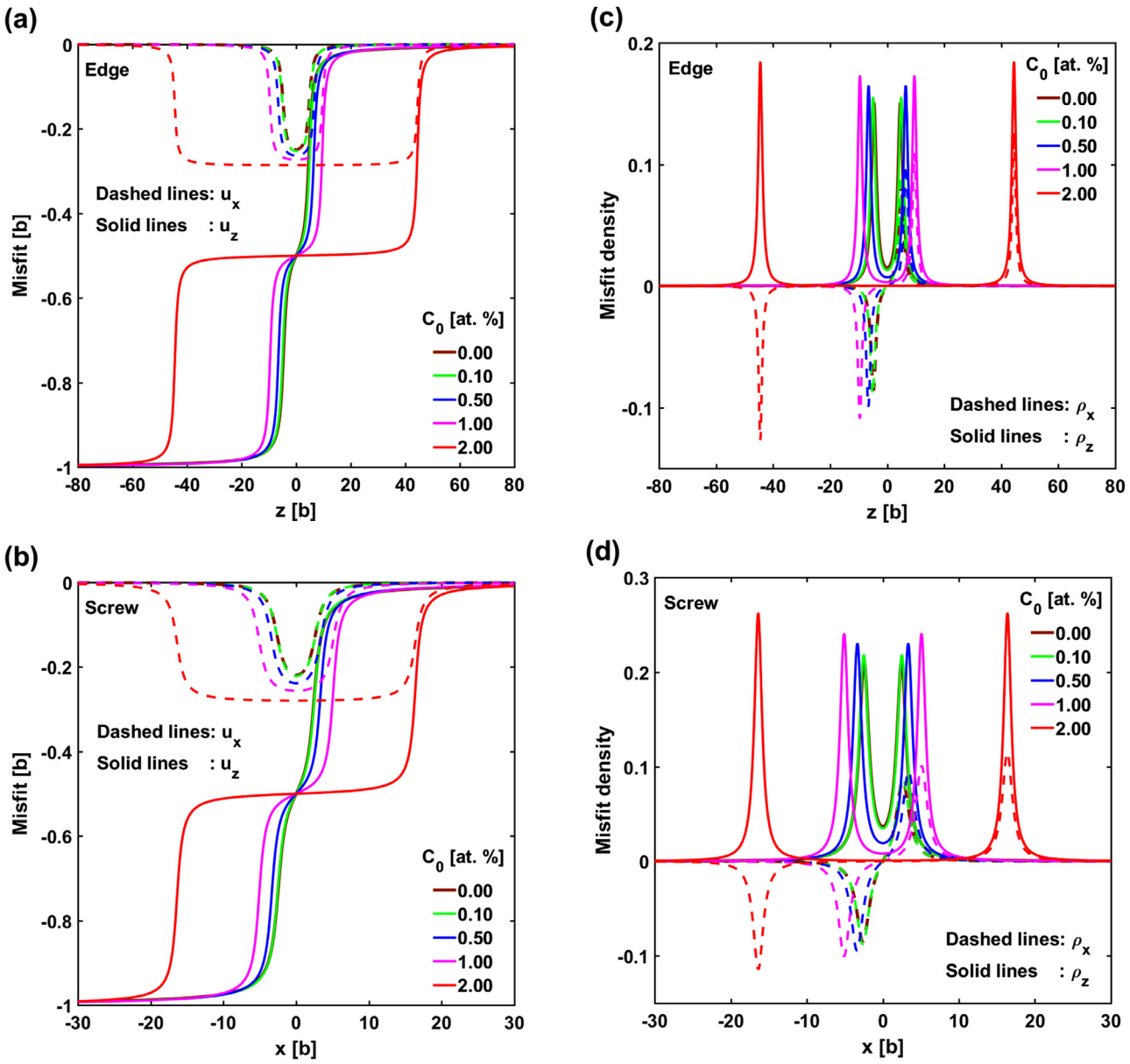


**Fig. 4.** The calculated misfit functions (a, b) and misfit densities (c, d) for the edge dislocation and screw dislocations at different bulk H concentrations $C_0$ without external stress applied, respectively. The dashed lines and the solid lines denote the components along the X-axis and the Z-axis, respectively.

function of Eq. (5), i.e. the positions of the edge ($x_e^{(i)}$) and screw ($x_s^{(i)}$) components of each partial dislocation ($i = 1, 2$), and the corresponding partial dislocation core widths ($w_e$ and $w_s$).

There are several assumptions and simplifications needed to be pointed out. First, when the generalized P–N model is used to obtain dislocation core structure, it is assumed that H atoms can move with the dislocation core simultaneously. This assumption should be true in two cases: one is that the dislocation velocity is low and the other is that H atoms can diffuse very fast. Second, the H distribution in the P–N model is assumed the same as the calculation of GSFE to simplify our calculation, as will be discussed below in Section 2.3. In this way, the H atoms mainly lie within the two atomic fault layers immediately adjacent the dislocation slip plane, which is a reasonable approximation due to the large atomic misfit around the dislocation core. Finally, the long-range H-dislocation interaction is neglected, since the H concentration within the dislocation core should be much higher than that outside the core, implying that H atoms inside the core may influence the dislocation mobility more heavily by short-range effect than those remote H atoms outside the core by long-range effect. In addition, the long-range interaction only operates at very high bulk H concentration and mainly affects the dislocation motion through the Peach–Kohler force. Therefore, only the short-range interaction is studied here, with an especial attention to the H effect on dislocation core structure.

### 2.3. The construction of H-affected γ-surfaces

As mentioned above, the misfit energy strongly depends on the γ-surface. The accuracy of the γ-surface under hydrogen circumstance is essential to the study of the H-affected dislocation core structure and the Peierls stress. To construct the γ-surface, it is necessary to calculate the stacking fault energies in the $< 112 >$ and $< 110 >$ directions, firstly. In the previous calculation of the stacking fault energies (Vítek, 1968), the simulation domain was divided into two halves by one {111} crystallographic plane. Then, the atoms in one half were shifted rigidly with respect to the other by a given fault vector in the $< 112 >$ or $< 110 >$ slip direction, following which the energy minimization was performed with all atoms allowed to relax only in the direction normal to the slip plane. However, in our computation, all

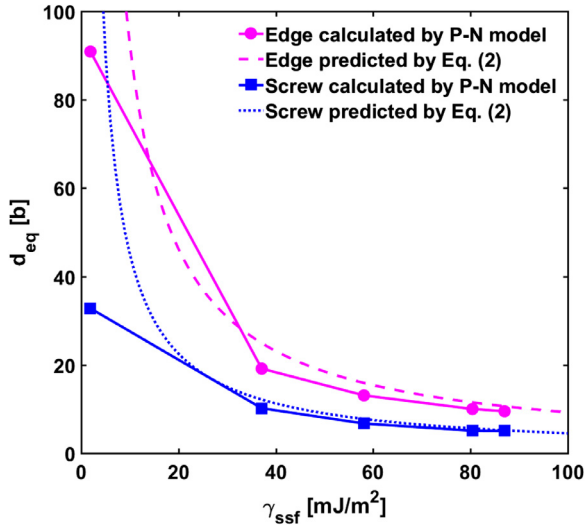


**Fig. 5.** The equilibrium separations between the dissociated two partials vs. the stable SFE. The dashed line and the dotted line denote the equilibrium separations for the edge dislocation and the screw one predicted by Eq. (2), respectively.

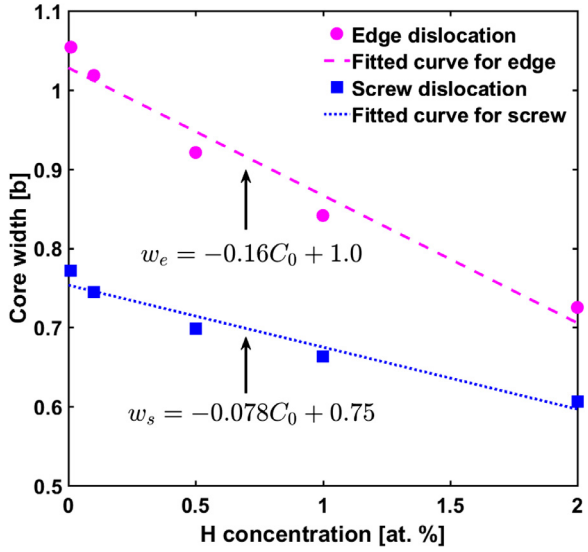


**Fig. 6.** The core width of an individual partial dislocation vs. the bulk H concentration. The circles and squares represent the numerical values, and the dashed line and dotted line denote the fitted curves, respectively.

atoms are also relaxed in the directions perpendicular to the shear direction, which doesn't influence the computational result of GSFE.

In previous studies, how the solute hydrogen affects GSFE is still in debate (Song et al., 2010; Tang and El-Awady, 2012). The main reason is that the migration and distribution of hydrogen atoms are dealt with in different ways in these stacking fault energy calculations. Inspired by Tang's method (Tang and El-Awady, 2012), the hydrogen migration is reasonably considered by investigating the stable interstitial sites of hydrogen atoms during the formation process of the stacking fault. In addition to the hydrogen atoms located within the two atomic stacking fault layers, those interstitial hydrogen atoms some distance away from the stacking fault layers, which also affect the stacking fault energy markedly, are considered as well. In order to connect the hydrogen distribution with the bulk hydrogen concentration $C_0$, the solute segregation model, which can effectively account for the hydrogen trapping, is adopted to introduce hydrogen atoms around the atomic fault layers (Zhu et al., 2018). When hydrogen atoms are introduced, they are allowed to move freely during the formation process of the stacking fault in order to move to the energy favorable interstitial sites. In this way, the stacking fault energy curves in the $< 112 >$ and $< 110 >$ directions with different bulk H concentrations can be obtained via a well-established EAM potential (Angelo et al., 1995). The details of the stacking fault energy calculation can be found in our another paper (Zhu et al., 2019).

With the computationally obtained stacking fault energy curves in the $< 112 >$ and $< 110 >$ directions, the γ-surface can be constructed by the Fourier series approximation $\gamma(\mathbf{u}) = \sum_{n=0}^{6} c_n f_n(\mathbf{u})$ (Schoeck, 2001), considering the rotational symmetry of the FCC lattice in {111} slip planes. In this way, the γ-surfaces with different bulk H concentrations are obtained as shown below.

### 2.4. The Peierls stress

As a straight dislocation glides on its slip plane, its core structure changes periodically due to the crystal lattice. As a result, the total energy of the dislocation also varies with its position. The position with the minimum total energy is a local stable site and is called the Peierls valley. The minimum energy needed to move this dislocation from one stable site to the next one is namely the Peierls barrier and the corresponding minimum resolved shear stress is called the Peierls stress, $\tau_p$.

The Peierls stress can be readily calculated from the P–N model in the following way: the glide stress that increases with an increment of 0.5 MPa is applied to the screw dislocation (or 0.01 MPa for the edge dislocation), and then the equilibrium core structure can be determined by minimizing the total energy of Eq. (7) with respect to the misfit functions of Eq. (5). With increasing glide stress, the equilibrium position of the dislocation changes as a result. A remarkable translation of the dislocation center occurs when the glide stress exceeds a critical value, implying that the Peierls barrier is overcome under this applied stress. Thus, this critical value can be identified as the Peierls stress.

### 2.5. The recombination energy

Dislocation cross-slip plays an important role in plastic deformation in metals (Püschl, 2002). In FCC crystals, a perfect screw dislocation does not have a definitive slip plane. It can easily glide from one slip plane to another. However, for an extended screw dislocation with edge components, cross-slip becomes difficult. In order to cross slip, it first recombines into a perfect screw dislocation on its original slip plane and then re-dissociates onto the cross-slip plane. The Escaig stress $\tau_{yx}$ can assist this process if it causes the partial dislocations to approach each other. At a critical value of the Escaig stress $\tau_{yx}^c$, the edge components annihilate with each other, and thus the two partial dislocations recombine into a perfect screw dislocation. Then, we can define the recombination energy as the difference between the total dislocation energy of Eq. (7) at the critical Escaig stress and zero stress, which can be regarded as an energy barrier for cross-slip of an extended screw dislocation (Szajewski et al., 2017):

$$\Delta E = E_{\text{total}}(\tau_{yx}^c) - E_{\text{total}}(0) \tag{11}$$

where $E_{\text{total}}(\tau_{yx}^c)$ is the total energy under recombined state, and $E_{\text{total}}(0)$ the total energy under extended state.

## 3. Main results

### 3.1. Effect of interstitial hydrogen on generalized stacking fault energy

In order to examine the effect of interstitial H on GSFE in Ni, we choose five different bulk H concentrations $C_0$ (in atomic ratio, at.%): 0, 0.1, 0.5, 1.0 and 2.0. Figs. 2(a) and (b) show the atomistic modeling results of GSFE along the $< 112 >$ and $< 110 >$ directions for the Ni-H system, respectively.

The GSFE profile along the $< 112 >$ direction has three

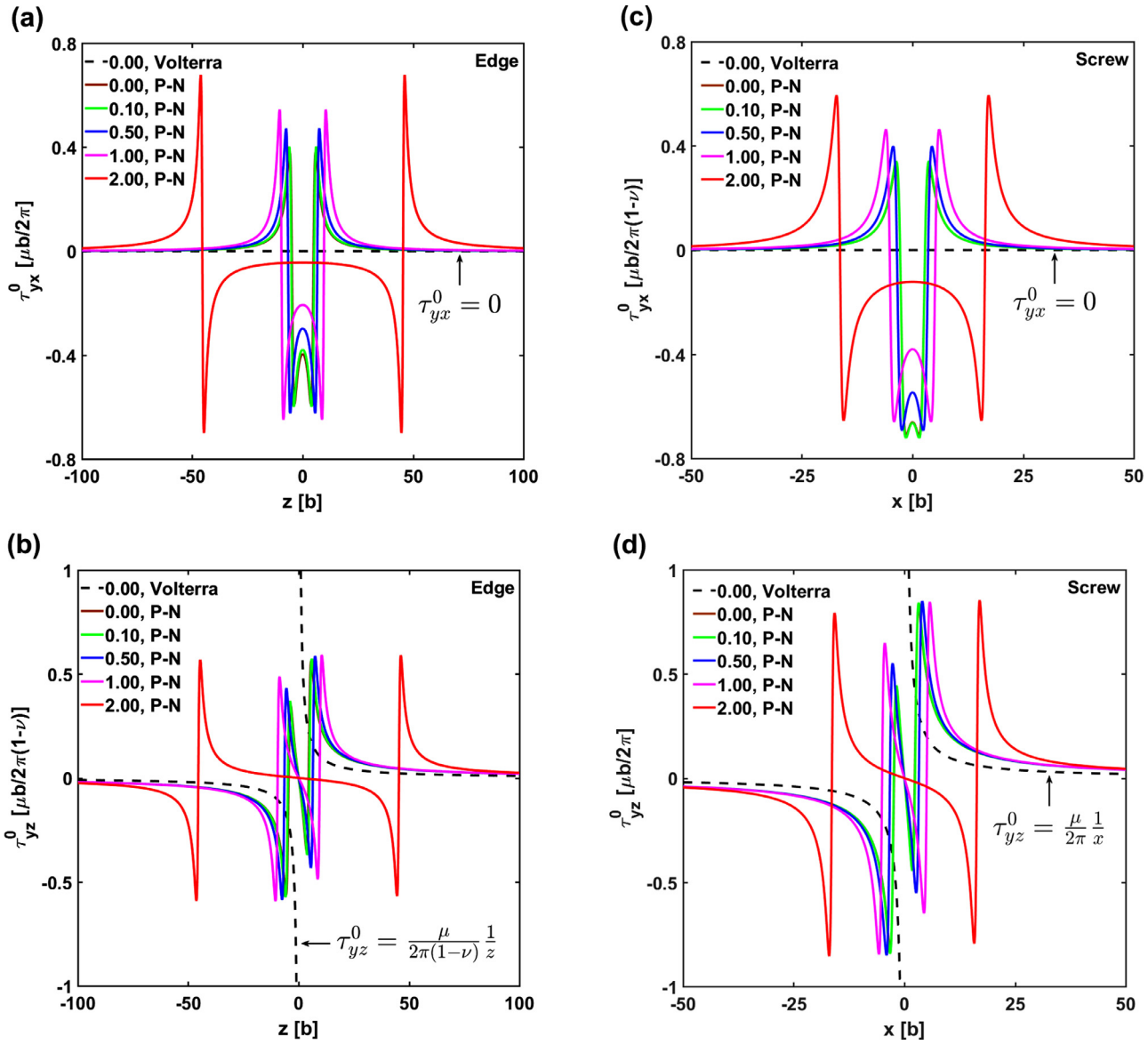


**Fig. 7.** The elastic stress field of $\tau^0_{yx}$ and $\tau^0_{yz}$ on the slip plane due to (a, b) the extended edge dislocation and (c, d) the extended screw dislocation at different bulk H concentrations.

characteristic values, which are the unstable stacking fault energy (SFE) $\gamma_{usf}$ that determines the energy barrier for nucleation of partial dislocations (Andric and Curtin, 2017; Rice, 1992), the stable SFE $\gamma_{ssf}$ that is associated with the SFW (Hirth and Lothe, 1992), and the maximum unstable SFE $\gamma_{mx}$, respectively. With the increase of H concentration from 0 to 2.0 (at.%), the stable SFE decreases from 87 mJ/m$^2$ to 2 mJ/m$^2$, while the unstable SFE increases from 212 mJ/m$^2$ to 259 mJ/m$^2$. Thus, both the energy barriers for nucleation of the leading partial ($\gamma_{usf}$) and the trailing partial ($\gamma_{usf} - \gamma_{ssf}$) are enhanced in the presence of H (Andric and Curtin, 2017; Rice, 1992). In addition, the maximum unstable SFE in both $< 112 >$ and $< 110 >$ directions decreases with increasing H concentration, as seen from Figs. 2(a) and (b).

In order to use the generalized P–N model to study the effect of interstitial H on the dislocation core structure quantitatively, we need first fit the $\gamma$-surfaces from the GSFE curves obtained above by atomic modeling. By using the Fourier series approximation (Schoeck, 2001), the $\gamma$-surfaces are fitted by the least-squares method. The fitted $\gamma$-surface at the hydrogen concentration of 1.0 (at.%) is plotted in Fig. 3(a), where the red circles represent GSFE curves calculated from atomistic modeling. As can be seen, the fitted result is satisfactory. Thus, the H-affected $\gamma$-surfaces obtained by this method can be used by the P–N model to quantify the effect of H on dislocation core structure. Fig. 3(b) shows the contour of GSFE with the illustration of the dissociation process of a perfect dislocation into two partial dislocations, where the red arrow denotes the perfect Burgers vector and the green arrows denote the Burgers vectors of partial dislocations, respectively.

### 3.2. Effect of interstitial hydrogen on the dislocation core structure

In order to demonstrate the validity of the generalized P–N model, we first calculate the equilibrium core structures for both edge and screw dislocations in the absence of H. The core structures are determined under zero applied stress. The equilibrium spacing between two partial dislocations can be obtained from the misfit function of Eq. (5) directly. From our calculated results, the equilibrium separation between partial dislocations of an extended edge dislocation is 9.56$b$ (23.80 Å), which is in reasonable agreement with atomistic calculation of 24.90 Å (Wen et al., 2005) and the predicted value of 10.63$b$ by Eq. (2). For an extended screw dislocation, the equilibrium spacing between the two partial dislocations is 5.17$b$ (12.87 Å), which is also

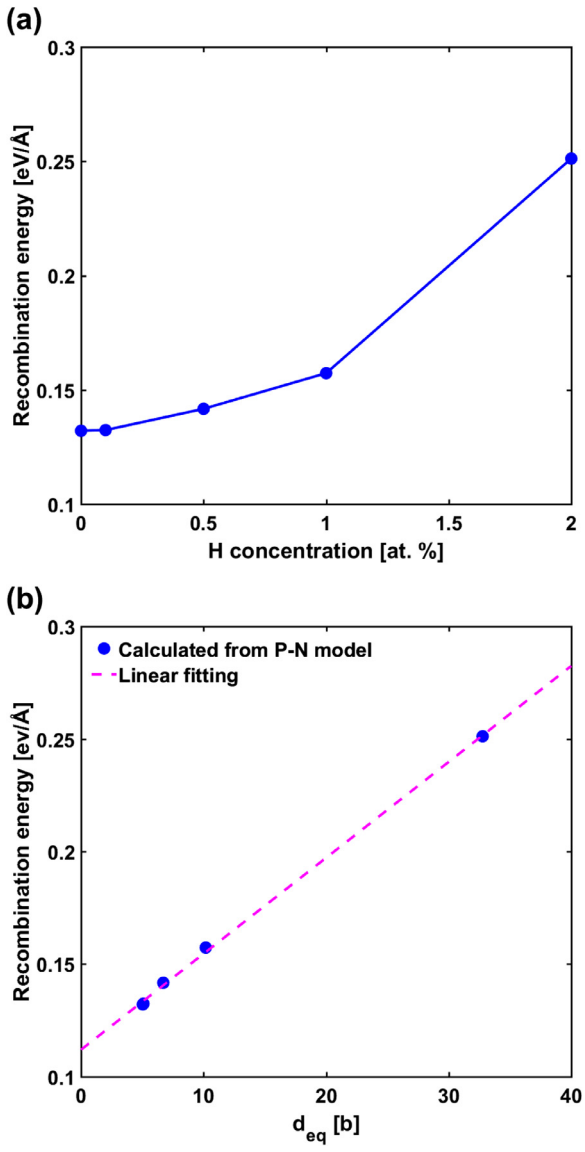


**Fig. 8.** (a) The recombination energy of the extended screw dislocation vs. bulk hydrogen concentration, and (b) the recombination energy vs. the equilibrium separation between partial dislocations.

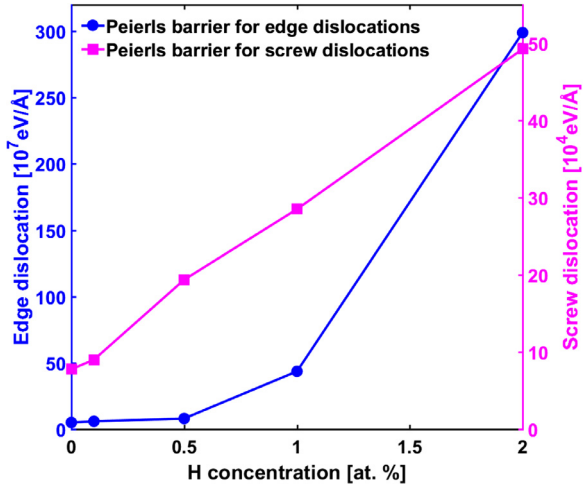


**Fig. 9.** The Peierls barrier of edge dislocation and screw dislocation vs. the bulk H concentration.

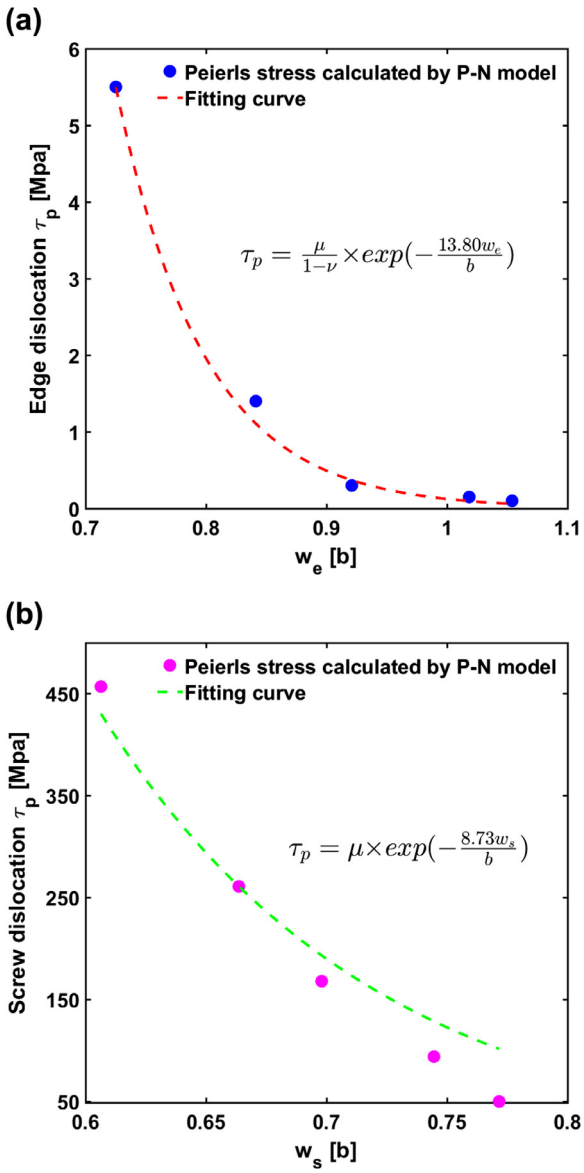


**Fig. 10.** The Peierls stress vs. the core width of the individual partial dislocation of (a) the extended edge dislocation and (b) the extended screw dislocation, respectively.

close to atomistic calculation of 14.50 Å (Wen et al., 2005) and the predicted value of 5.18*b* by Eq. (2). Thus, the generalized P–N model is suitable for the straight dislocations.

With the help of the H-affected γ-surfaces, the misfit energy can be obtained by Eq. (9). By minimizing energy of Eq. (7) without external force, the misfit function and its derivative (the misfit density) that characterize the core structure of a straight dislocation can then be determined in the presence of H. The long-range elastic interaction between dislocation and H is neglected, since the highest bulk H concentration in our calculation is 2.0 (at.%), which is still a low concentration for the operating of H shielding mechanism (Song et al., 2019; von Pezold et al., 2011). Moreover, the long-range interaction mainly affects the dislocation motion through the Peach-Koehler force rather than through changing the dislocation core (Cai et al., 2014; Sofronis, 1995).

Fig. 4(a) and (b) are the resultant misfit functions of edge and screw dislocations at different bulk H concentrations without external stress, while Fig. 4(c) and (d) are the corresponding misfit densities. The dashed lines denote the components along the X-axis and the solid lines

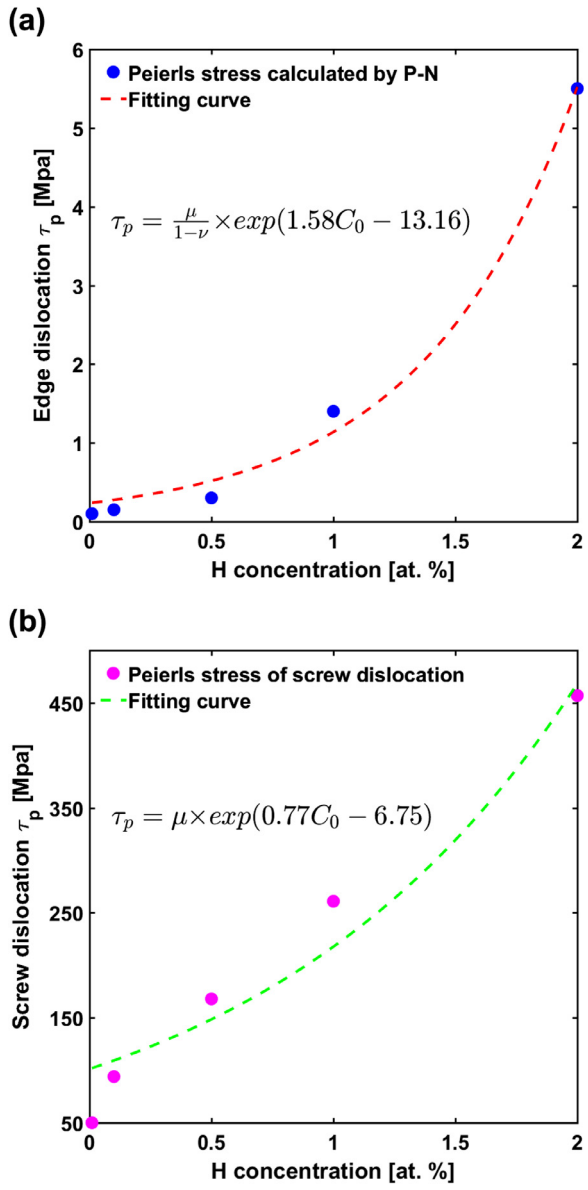


**Fig. 11.** The Peierls stress vs. the bulk H concentration for (a) the edge dislocation and (b) the screw dislocation, respectively.

denote the components along the Z-axis, respectively. There are two characteristic lengths that can be used to describe the core structures of an extended dislocation. One is the equilibrium spacing between the two partial dislocations, $d_{eq}$, which is intimately related to the activation energy for cross-slip (Püschl, 2002). The other is the peak value of the misfit density, which determines the energy barrier for nucleating a partial dislocation (Andric and Curtin, 2017; Rice, 1992). It is clear from Fig. 4 that H can enhance the equilibrium separations $d_{eq}$ for both extended edge and screw dislocations, which can be mainly attributed to the decrease of the stable SFE. As shown in Fig. 4(c) and (d), the peak values in the misfit density profile increase with increasing H concentration, which are mainly due to the increase of the unstable SFE. As some researchers pointed out, increasing peak values indicate that the nucleation of partial dislocations becomes difficult (Andric and Curtin, 2017; Rice, 1992). Therefore, H could inhibit the nucleation of partial dislocation, which is consistent with the recent experimental observations in Ag (Yin et al., 2019).

Fig. 5 shows the equilibrium spacing of extended edge and screw dislocations vs. the stable SFE. When the stable SFE is higher than 40 mJ/m$^2$, the equilibrium spacing calculated by the P–N model is close to the predictions of Eq. (2). However, when the stable SFE approaches zero, the equilibrium spacing predicted by Eq. (2) deviates seriously from that by the P–N model. That is, the Volterra model seems not suitable for predicting the equilibrium spacing of dislocation in the H-charged Ni with low stable SFE. The underlying reason is that the equilibrium spacing also depends on the unstable SFE besides the stable SFE (Kibey et al., 2006), of which both are included in our P–N model. It should be pointed out, although the equilibrium spacing increases with increasing H concentration, the core width of each individual partial dislocation decreases almost linearly with the increase of H concentration, as shown in Fig. 6. The increase of the core width of partial dislocations can strongly affect its glide resistance as discussed below.

As indicated by Eq. (6), the dislocation stress field depends closely on its core structure, so the H-affected dislocation core structure can affect the dislocation stress field indirectly. Once the core structure is obtained, the P–N model gives the elastic stress field of an extended screw dislocation by Eq. (6). The elastic stress field of an extended edge dislocation can also be deduced with minor changes, i.e. the misfit function $\mathbf{u}(x)$ should be replaced by $\mathbf{u}(z)$ due to the change of dislocation line direction. Fig. 7 shows the elastic stress field of both extended edge and screw dislocations on their slip plane at different bulk H concentrations. The stress field at the H concentration of 0.1 (at.%) almost coincides with that in the absence of H, due to their similar core structures. As shown in Fig. 7, hydrogen mainly affects the stress field within the core region, due to the strong interaction between dislocation core and hydrogen. Outside the core region, the stress field can be well described by the solution of the Volterra dislocation (Hirth and Lothe, 1992), which are shown by the dashed curves in Fig. 7.

### 3.3. Effect of interstitial hydrogen on dislocation cross-slip

Many experimental results indicated that the solute hydrogen had strong effect on the screw dislocation motion, inhibiting its cross-slip behavior and resulting in the slip planarity (Robertson, 1999; Wen et al., 2004). By considering the hydrogen effect on the recombination energy of an extended screw dislocation, the cross-slip behavior of screw dislocation in the H-charged Ni is quantitatively studied here. Utilizing the generalized P–N model, the critical Escaig stress ($\tau^c_{yx}$), at which the extended screw dislocation can be recombined by annihilating the edge components of partial dislocations with each other ($u_x = 0$), can be determined. Then, the recombination energy can be calculated by Eq. (11) as the difference in dislocation energy between recombined state and extended state, which can be regarded as the energy barrier for cross-slip. As shown in Fig. 8(a), with the increase of H concentration, the recombination energy for the extended screw dislocation increases, indicating that H can suppress screw dislocation cross-slip and thus facilitate slip planarity. This result is consistent with experiments (Robertson, 1999) and atomistic calculations (Wen et al., 2004). As shown in Fig. 8(b), the recombination energy increases almost linearly with the equilibrium separations between partial dislocations of the extended screw dislocation. One explanation is that the reduction of the stable SFE due to interstitial H results in wider equilibrium spacing between partial dislocations and thus increases the difficulty of the recombination process.

On the other hand, to further investigate the role of H in cross-slip, we calculate the so-called binding energy of H to dislocation as the difference of dislocation energy with and without H following Lu et al (2001):

$$E_{bind} = (E^H_{elastic} + E^H_{misfit}) - (E^{no-H}_{elastic} + E^{no-H}_{misfit}) \quad (12)$$

This so-called binding energy is slightly different from the binding energy in common sense, because the constant energy term of hydrogen in bulk is neglected. However, it can still reflect the strength of hydrogen bound to dislocation.

For an extended screw dislocation, each of the two partial dislocations is a mixed dislocation. Since the binding energy of H to dislocation relates to the dislocation character, it can influence the recombination of the screw dislocation directly. Our calculations show that H can reduce the dislocation energy due to negative binding energy of H to dislocation. Taking the case of H concentration of 1.0 (at.%) for example, the binding energies are -0.064 eV/Å for the edge dislocation and − 0.022 eV/Å for the screw dislocation, respectively. Obviously, the binding energy of H to the edge dislocation is approximately three times larger than that to the screw dislocation, which indicates that hydrogen can stabilize the edge components of an extended screw dislocation. Since cross-slip of an extended screw dislocation involves its edge components annihilation with each other, the cross-slip becomes difficult in H environment (Wen et al., 2004). It seems that the hydrogen-enhanced slip planarity is a coaction of the stable SFE and H-dislocation binding energy.

### 3.4. Effect of interstitial hydrogen on the Peierls stress

By using the generalized P–N model, the equilibrium core structures of a straight dislocation at different positions can be obtained. Due to the periodicity of the lattice, the total energy of a straight dislocation is a periodic function of its position. The Peierls barrier is defined as the difference between the maximum dislocation energy and the minimum one when changing the dislocation position. In the absence of H, the Peierls barriers are $5.11 \times 10^7$eV/Å for the edge dislocation and $7.76 \times 10^4$eV/Å for the screw dislocation, which are on the same order as Wen's full-scale atomistic simulation results, i.e. $1.30 \times 10^6$eV/Å for the edge dislocation and $1.62 \times 10^4$eV/Å for the screw dislocation (Wen et al., 2005). As shown in Fig. 9, the Peierls barriers for both edge and screw dislocations increase with increasing H concentration, indicating that H can hinder the dislocation motion on its slip plane to some extent.

The Peierls stress, corresponding to the minimum shear stress to move a straight dislocation rigidly at zero temperature, can be obtained as mentioned in Section 2.4. In the absence of H, the Peierls stress calculated from the generalized P–N model is 0.15 MPa for the edge dislocation, which is close to the atomistic modeling value of 0.21 MPa (Wen et al., 2005). For the screw dislocation, the calculated Peierls stress is 50 MPa, which is approximately three times larger than the atomistic calculation of 15 MPa (Wen et al., 2005). The large difference may come from the non-local atomic interactions in the core region, which are neglected in the P–N model for simplicity (Liu et al., 2017). Since we mainly focus on the interaction between dislocation and interstitial hydrogen, the non-local atomic interaction should not remarkably affect the overall results.

For a perfect straight edge dislocation with sinusoidal misfit energy, the Peierls stress is usually described as (Joós and Duesbery, 1997)

$$\tau_p = \frac{\mu}{1-\nu}\exp\left(-\frac{2\pi w}{b}\right) \tag{13}$$

where $w$ is core width of the dislocation. For the case of screw dislocations, the term $(1-\nu)$ in Eq. (13) should be replaced by unity. In Eq. (13), we see the Peierls stress decreases with the increase of the core width. For an extended dislocation, if the two partial dislocations are well separated, each of them only needs to overcome its own Peierls barrier during glide (Schoeck and Püschl, 1994). In other words, the Peierls stress of an extended dislocation is just the Peierls stress of each partial. For an extended dislocation in Ni, the equilibrium separation of the two partial dislocations is large enough to satisfy the above assumption. Fig. 10 shows the variation of the Peierls stress with the core width of the partial dislocation. The Peierls stress decreases with the increase of the core width of an individual partial dislocation. Motivated by Eq. (13), it is fitted by the equation as:

$$\tau_p = \frac{\mu}{1-\nu}\exp\left(-\frac{\mathrm{A}w}{b}\right) \tag{14}$$

where A is a fitting parameter. Similarly, the term (1-$\nu$) in Eq. (14) should be set to unity for screw dislocations. From our calculations, A is 13.80 for the edge dislocations and 8.73 for the screw dislocations, respectively.

As mentioned in Section 3.2, the core width of the partial dislocation decreases with the increase of H concentration as shown in Fig. 6, indicating that the Peierls stress increases with the increases of H concentration. The Peierls stress vs. H concentration is plotted in Fig. 11. From the curves, the calculated Peierls stress indeed increases with increasing H concentration for both extended edge and screw dislocations. That is to say, H acts as an obstacle to dislocation motion along its slip plane. This result is contrary to that of Lu et al. (2001), where a H effect on the unstable SFE contrary to Tang et al.'s and our calculations (Tang and El-Awady, 2012). To be pointed out, the interaction between dislocations and hydrogen in the present P–N model is short-range, which is clearly different from the long-range interaction that interstitial H could shield the elastic interaction between dislocations and obstacles (Cai et al., 2014; Sofronis, 1995; Song et al., 2019). Using the linear dependence of the core width of partial dislocations on the H concentration shown in Fig. 6, the Peierls stress vs. the H concentration can be fitted by the following formula:

$$\tau_p = \frac{\mu}{1-\nu}\exp(pC_0 + q) \tag{15}$$

where $p$ and $q$ are fitting parameters. For the edge dislocations, $p = 1.58$ and $q = -13.6$. For the screw dislocations, $p = 0.77$and $q = 6.75$. These fitting relations may be used for the discrete dislocation dynamics (DDD) simulation and dislocation-density based crystal plasticity (CP) modeling (Hou et al., 2008; Huang and Li, 2015; Yuan et al., 2019).

## 4. Conclusions and discussions

In this work, an atomistically-informed generalized P–N model is employed to study the effects of interstitial H on the dislocation core structure, the recombination energy of extended screw dislocation and the Peierls stress in Ni. The main conclusions are summarized as follow:

- The unstable SFE increases with increasing H concentration, resulting in the increase of maximum misfit density. The increase of maximum misfit density, which is a key quantity describing the energy barrier for nucleation of a partial dislocation, implies that H can inhibit partial dislocation nucleation.
- The P–N model predicts that H can enhance the SFW of an extended dislocation but decease the core width of each partial dislocation. The SFW of the extended dislocation strongly depends on the H-affected stable SFE. The core width of each partial dislocation changes almost linearly with the H concentration. Thereby the dislocation stress fields are changed indirectly by solute H.
- The recombination energy of the extended screw dislocation increases with increasing H concentration, due to the coaction of the stable SFE and the H-dislocation binding energy. As a result, H can suppress the cross-slip of an extended screw dislocation and facilitate its slip planarity.
- The Peierls stress increases with increasing H concentration, implying those H atoms trapped at dislocation core can serve as obstacles to dislocation motion. This can be ascribed to a reduction in the core width of each partial dislocation due to the solute H. The H-affected Peierls stress can be obtained by a modified classical Peierls stress formula, which can be used for the DDD simulations and CP modeling.

What needs to be pointed out in particular is that only the short-range H-dislocation interaction is studied here, with an especial

attention to the H effect on dislocation core structure. A basic conclusion is that H hinders dislocation motion to some extent by changing dislocation core structure. It is contrary to the hydrogen shielding effect on dislocation due to the long-range H-dislocation interaction. In practice, both long-range and short-range interactions exist simultaneously, which of them dominate depends on several factors, such as H concentration, dislocation type, GSFE, and so on. In the H-affected DDD simulations, these two interactions should be appropriately considered.

## Declaration of Competing Interest

The authors declare that they have no known competing financial interests or personal relationships that could have appeared to influence the work reported in this paper.

## Acknowledgements

This work was financially supported by National Natural Science Foundation of China (Grant no. 11632007, 11802099 and 11572136).

## Supplementary materials

Supplementary material associated with this article can be found, in the online version, at doi:10.1016/j.mechmat.2019.103221.

## References

Andric, P., Curtin, W.A., 2017. New theory for Mode I crack-tip dislocation emission. J. Mech. Phys. Solids 106, 315–337. https://doi.org/10.1016/j.jmps.2017.06.006.

Angelo, J.E., Moody, N.R., Baskes, M.I., 1995. Trapping of hydrogen to lattice defects in nickel. Model. Simul. Mater. Sci. Eng. 3, 289–307. https://doi.org/10.1088/0965-0393/3/3/001.

Barrera, O., Bombac, D., Chen, Y., Daff, T.D., Galindo-Nava, E., Gong, P., Haley, D., Horton, R., Katzarov, I., Kermode, J.R., Liverani, C., Stopher, M., Sweeney, F., 2018. Understanding and mitigating hydrogen embrittlement of steels: a review of experimental, modelling and design progress from atomistic to continuum. J. Mater. Sci. 53, 6251–6290. https://doi.org/10.1007/s10853-017-1978-5.

Bulatov, V.V., Cai, W., 2006. Computer Simulations of Dislocations. Oxford University Press.

Bulatov, V.V., Kaxiras, E., 1997. Semidiscrete variational Peierls framework for dislocation core properties. Phys. Rev. Lett. 78, 4221–4224. https://doi.org/10.1103/PhysRevLett.78.4221.

Cai, W., Sills, R.B., Barnett, D.M., Nix, W.D., 2014. Modeling a distribution of point defects as misfitting inclusions in stressed solids. J. Mech. Phys. Solids 66, 154–171. https://doi.org/10.1016/j.jmps.2014.01.015.

Cottrell, A.H., Bilby, B.A., 1949. Dislocation theory of yielding and strain ageing of iron. Proc. Phys. Soc. Sect. A 62, 49–62. https://doi.org/10.1088/0370-1298/62/1/308.

Eshelby, J.D., 1949. LXXXII. Edge dislocations in anisotropic materials. Philos. Mag. 40, 903–912. https://doi.org/10.1080/14786444908561420.

Ferreira, P.J., Robertson, I.M., Birnbaum, H.K., 1998. Hydrogen effects on the interaction between dislocations. Acta Mater. 46, 1749–1757. https://doi.org/10.1016/S1359-6454(97)00349-2.

Gahr, S., Grossbeck, M.L., Birnbaum, H.K., 1977. Hydrogen embrittlement of Nb I—Macroscopic behavior at low temperatures. Acta Metall. 25, 125–134. https://doi.org/10.1016/0001-6160(77)90116-X.

Hirth, J.P., Lothe, J., 1992. Theory of Dislocations, 2nd ed. Krieger Publishing Company.

Hou, C., Li, Z., Huang, M., Ouyang, C., 2008. Discrete dislocation plasticity analysis of single crystalline thin beam under combined cyclic tension and bending. Acta Mater 56, 1435–1446. https://doi.org/10.1016/j.actamat.2007.11.032.

Huang, M., Li, Z., 2015. Coupled DDD–FEM modeling on the mechanical behavior of microlayered metallic multilayer film at elevated temperature. J. Mech. Phys. Solids 85, 74–97. https://doi.org/10.1016/j.jmps.2015.09.007.

Itakura, M., Kaburaki, H., Yamaguchi, M., Okita, T., 2013. The effect of hydrogen atom on the screw dislocation mobility in bcc iron: a first-principles study. Acta Mater 61, 6857–6867. https://doi.org/10.1016/j.actamat.2013.07.064.

Johnson, W.H., 1875. On some remarkable changes produced in iron and steel by the action of hydrogen and acids. Proc. R. Soc. Lond. 23, 168–179. https://doi.org/10.1098/rspl.1874.0024.

Joós, B., Duesbery, M.S., 1997. The Peierls stress of dislocations: an analytic formula. Phys. Rev. Lett. 78, 266–269. https://doi.org/10.1103/PhysRevLett.78.266.

Kibey, S., Liu, J.B., Curtis, M.J., Johnson, D.D., Sehitoglu, H., 2006. Effect of nitrogen on generalized stacking fault energy and stacking fault widths in high nitrogen steels. Acta Mater 54, 2991–3001. https://doi.org/10.1016/j.actamat.2006.02.048.

Li, S., Li, Y., Lo, Y.-.C., Neeraj, T., Srinivasan, R., Ding, X., Sun, J., Qi, L., Gumbsch, P., Li, J., 2015. The interaction of dislocations and hydrogen-vacancy complexes and its importance for deformation-induced proto nano-voids formation in α-Fe. Int. J. Plast. 74, 175–191. https://doi.org/10.1016/j.ijplas.2015.05.017.

Liu, G., Cheng, X., Wang, J., Chen, K., Shen, Y., 2017. Improvement of nonlocal Peierls-Nabarro models. Comput. Mater. Sci. 131, 69–77. https://doi.org/10.1016/j.commatsci.2017.01.038.

Lu, G., Zhang, Q., Kioussis, N., Kaxiras, E., 2001. Hydrogen-enhanced local plasticity in aluminum: an ab initio study. Phys. Rev. Lett. 87, 095501. https://doi.org/10.1103/PhysRevLett.87.095501.

Martin, M.L., Somerday, B.P., Ritchie, R.O., Sofronis, P., Robertson, I.M., 2012. Hydrogen-induced intergranular failure in nickel revisited. Acta Mater. 60, 2739–2745. https://doi.org/10.1016/j.actamat.2012.01.040.

Nabarro, F.R.N., 1947. Dislocations in a simple cubic lattice. Proc. Phys. Soc. 59, 256–272. https://doi.org/10.1088/0959-5309/59/2/309.

Nagao, A., Dadfarnia, M., Somerday, B.P., Sofronis, P., Ritchie, R.O., 2018. Hydrogen-enhanced-plasticity mediated decohesion for hydrogen-induced intergranular and "quasi-cleavage" fracture of lath martensitic steels. J. Mech. Phys. Solids 112, 403–430. https://doi.org/10.1016/j.jmps.2017.12.016.

Nagumo, M., Takai, K., 2019. The predominant role of strain-induced vacancies in hydrogen embrittlement of steels: overview. Acta Mater. 165, 722–733. https://doi.org/10.1016/j.actamat.2018.12.013.

Oriani, R., 1970. The diffusion and trapping of hydrogen in steel. Acta Metall 18, 147–157. https://doi.org/10.1016/0001-6160(70)90078-7.

Oriani, R.A., Josephic, P.H., 1974. Equilibrium aspects of hydrogen-induced cracking of steels. Acta Metall 22, 1065–1074. https://doi.org/10.1016/0001-6160(74)90061-3.

Peierls, R., 1940. The size of a dislocation. Proc. Phys. Soc. 52, 34–37. https://doi.org/10.1088/0959-5309/52/1/305.

Püschl, W., 2002. Models for dislocation cross-slip in close-packed crystal structures: a critical review. Prog. Mater. Sci. 47, 415–461. https://doi.org/10.1016/S0079-6425(01)00003-2.

Rice, J.R., 1992. Dislocation nucleation from a crack tip: an analysis based on the Peierls concept. J. Mech. Phys. Solids 40, 239–271. https://doi.org/10.1016/S0022-5096(05)80012-2.

Robertson, I.M., 1999. The effect of hydrogen on dislocation dynamics. Eng. Fract. Mech. 64, 649–673. https://doi.org/10.1016/S0013-7944(99)00094-6.

Robertson, I.M., Sofronis, P., Nagao, A., Martin, M.L., Wang, S., Gross, D.W., Nygren, K.E., 2015. Hydrogen embrittlement understood. Metall. Mater. Trans. A 46, 2323–2341. https://doi.org/10.1007/s11661-015-2836-1.

Schoeck, G., 2005. The Peierls model: progress and limitations. Mater. Sci. Eng. A 400–401, 7–17. https://doi.org/10.1016/j.msea.2005.03.050.

Schoeck, G., 2001. The core structure, recombination energy and Peierls energy for dislocations in Al. Philos. Mag. A 81, 1161–1176. https://doi.org/10.1080/01418610108214434.

Schoeck, G., Püschl, W., 1994. Dissociated dislocations in the Peierls potential. Mater. Sci. Eng. A 189, 61–67. https://doi.org/10.1016/0921-5093(94)90401-4.

Sharma, S., Ghoshal, S.K., 2015. Hydrogen the future transportation fuel: from production to applications. Renew. Sustain. Energy Rev. 43, 1151–1158. https://doi.org/10.1016/j.rser.2014.11.093.

Sofronis, P., 1995. The influence of mobility of dissolved hydrogen on the elastic response of a metal. J. Mech. Phys. Solids 43, 1385–1407. https://doi.org/10.1016/0022-5096(95)00037-J.

Song, J., Curtin, W.A., 2014. Mechanisms of hydrogen-enhanced localized plasticity: an atomistic study using α-Fe as a model system. Acta Mater. 68, 61–69. https://doi.org/10.1016/j.actamat.2014.01.008.

Song, J., Soare, M., Curtin, W.A., 2010. Testing continuum concepts for hydrogen embrittlement in metals using atomistics. Model. Simul. Mater. Sci. Eng. 18, 045003. https://doi.org/10.1088/0965-0393/18/4/045003.

Song, Q., Zhu, Y., Huang, M., Li, Z., 2019. Shielding or anti-shielding effects of solute hydrogen near a finite length crack: a new possible mechanism of hydrogen embrittlement. Mech. Mater. 132, 109–120. https://doi.org/10.1016/j.mechmat.2019.02.015.

Szajewski, B.A., Hunter, A., Beyerlein, I.J., 2017. The core structure and recombination energy of a copper screw dislocation: a Peierls study. Philos. Mag. 97, 2143–2163. https://doi.org/10.1080/14786435.2017.1328138.

Szajewski, B.A., Hunter, A., Luscher, D.J., Beyerlein, I.J., 2018. The influence of anisotropy on the core structure of Shockley partial dislocations within FCC materials. Model. Simul. Mater. Sci. Eng. 26, 015010. https://doi.org/10.1088/1361-651X/aa9758.

Tang, Y., El-Awady, J.A., 2012. Atomistic simulations of the interactions of hydrogen with dislocations in fcc metals. Phys. Rev. B 86, 174102. https://doi.org/10.1103/PhysRevB.86.174102.

Vítek, V., 1968. Intrinsic stacking faults in body-centred cubic crystals. Philos. Mag. 18, 773–786. https://doi.org/10.1080/14786436808227500.

von Pezold, J., Lymperakis, L., Neugebeauer, J., 2011. Hydrogen-enhanced local plasticity at dilute bulk H concentrations: the role of H–H interactions and the formation of local hydrides. Acta Mater. 59, 2969–2980. https://doi.org/10.1016/j.actamat.2011.01.037.

Wang, S., Martin, M.L., Sofronis, P., Ohnuki, S., Hashimoto, N., Robertson, I.M., 2014. Hydrogen-induced intergranular failure of iron. Acta Mater. 69, 275–282. https://doi.org/10.1016/j.actamat.2014.01.060.

Wen, M., Fukuyama, S., Yokogawa, K., 2004. Hydrogen-affected cross-slip process in fcc nickel. Phys. Rev. B 69, 174108. https://doi.org/10.1103/PhysRevB.69.174108.

Wen, M., Ngan, A.H.W., Fukuyama, S., Yokogawa, K., 2005. Full-scale atomistic simulations of dislocations in Ni crystal by embedded-atom method. Philos. Mag. 85, 1917–1929. https://doi.org/10.1080/14786430500070966.

Xie, D., Li, S., Li, M., Wang, Z., Gumbsch, P., Sun, J., Ma, E., Li, J., Shan, Z., 2016. Hydrogenated vacancies lock dislocations in aluminium. Nat. Commun. 7, 13341. https://doi.org/10.1038/ncomms13341.

Yin, S., Cheng, G., Chang, T.-.H., Richter, G., Zhu, Y., Gao, H., 2019. Hydrogen

embrittlement in metallic nanowires. Nat. Commun. 10, 2004. https://doi.org/10.1038/s41467-019-10035-0.

Yuan, S., Zhu, Y., Liang, S., Huang, M., Li, Z., 2019. Dislocation-density based size-dependent crystal plasticity framework accounting for climb of piled up dislocations at elevated temperature. Mech. Mater. 134, 85–97. https://doi.org/10.1016/j.mechmat.2019.04.015.

Zhu, Y., Li, Z., Huang, M., Fan, H., 2017. Study on interactions of an edge dislocation with vacancy-H complex by atomistic modelling. Int. J. Plast. 92, 31–44. https://doi.org/10.1016/j.ijplas.2017.03.003.

Zhu, Y., Li, Z., Huang, M., Xiong, Q., 2018. The shock response of crystalline Ni with H-free and H-segregated ⟨1 1 0⟩ symmetric tilt GBs. Comput. Mater. Sci. 147, 258–271. https://doi.org/10.1016/j.commatsci.2018.02.030.

Zhu, Y., Zheng, Z., Liang, S., Li, Z., Huang, M., 2019. Modeling of solute hydrogen effect on various planar fault energies. Under review.